Synthesis, characterization and photophysics of new photoactive ESIPT lipophilic dyes. Partition experiments with different composed liposomes

ARTICLE *in* DYES AND PIGMENTS · NOVEMBER 2014

Impact Factor: 3.97 · DOI: 10.1016/j.dyepig.2014.04.024

3 AUTHORS, INCLUDING:

Fabiano Severo Rodembusch
Universidade Federal do Rio Grande do Sul
10 PUBLICATIONS **3** CITATIONS
SEE PROFILE

Leandra Franciscato Campo
Universidade Federal do Rio Grande do Sul
34 PUBLICATIONS **330** CITATIONS
SEE PROFILE

Dyes and Pigments 110 (2014) 134–142

Contents lists available at ScienceDirect

Dyes and Pigments

journal homepage: www.elsevier.com/locate/dyepig

Synthesis, characterization and photophysics of new photoactive ESIPT lipophilic dyes. Partition experiments with different composed liposomes

Felipe Lange Coelho, Fabiano Severo Rodembusch*, Leandra Franciscato Campo*

Grupo de Pesquisa em Novos Materiais Orgânicos e Fotoquímica, Instituto de Química, Departamento de Química Orgânica, Universidade Federal do Rio Grande do Sul, UFRGS, CEP 91501-970 Porto Alegre, RS, Brazil

ARTICLE INFO

Article history:
Received 2 March 2014
Received in revised form
8 April 2014
Accepted 16 April 2014
Available online 24 April 2014

Keywords:
Fluorescent probes
Liposome
Ethosome
Membrane probes
Lipophilic dyes
ESIPT

ABSTRACT

New lipophilic dyes were synthesized from a fluorescent precursor and used to produce photoactive liposomes and ethosomes made of different phospholipids. The lipophilic dyes absorbed in the ultraviolet region due to π–π* transitions and had a dual fluorescence emission in the violet–yellow regions, depending on solvent polarity. The long alkyl chain lipophilic dyes had a narrow emission band with a very regular shape, and their photophysical behaviour indicates that these dyes were inserted into the lipid bilayer. The dye with short alkyl chain appeared to be in a polar environment, which indicated this fluorophore experienced a more hydrophobic environment. Fluorescence titration experiments were also performed with this compound and the partition coefficient was determined, which showed higher values than those found in the literature for similar intramolecular proton transfer dyes, likely due to better interaction between this dye and the phospholipids, due to the alkyl chain present in the dyes.

1. Introduction

Since the discovery by Bangham et al. which showed that phospholipids could self-assemble in aqueous solutions to form highly-organized structures (liposomes) [1], the interest in these artificially-prepared vesicles has increased considerably due to their properties. Liposomes are defined as microscopic spherical-shaped vesicles formed by one or more multiple concentric phospholipid bilayers composed with an aqueous interior, which allow interaction with hydrophilic or hydrophobic molecules by encapsulation in the aqueous interior or entrapment within the lipid bilayer, respectively [2]. Liposomes can have differential permeability, where low-polarity molecules tend to partition into interior more readily, and thus permeate faster. On the other hand, polar compounds permeate the membrane more slowly, and very polar solutes do not permeate at all (over several minutes) [3]. Additionally, these structures can also present high chemical and physical stability [4]. Based on these properties, liposomes can mimic cell membranes [5], as liposomes and cell membranes have very similar composition, shape, chemical and physical properties [6,7], which allow for the extension of results obtained in liposomes to cell membranes [8].

Fluorescence spectroscopy has been extensively applied since the late 1960s to study different aspects of membrane-related phenomena [9–11]. This technique provides information about the organization, motion and surface of the membrane, which helps understand the motion of fatty acyl chains, the dynamics of phospholipids in the bilayer(s), as well as the distribution and orientation of lipids and other components [12–18]. Furthermore, some fluorescent features, such as a large Stokes' shift, stable fluorescence emission as well as thermal and photochemical stability [9,19] are needed to design new fluorescent membrane probes; excited state intramolecular proton transfer (ESIPT) compounds well fit these requirements [20,21]. The ESIPT mechanism is due to the absorption of radiation from an enol-*cis* conformer (^{1}E), which is usually the most stable conformer in the ground state (solution or solid state). In the excited state, this conformer undergoes ESIPT to form a keto tautomer (^{1}K*) giving rise to an emission with a large Stokes' shift. Additional conformers such as the enol open structure (Fig. 1, right) do not undergo ESIPT [22]. These non ESIPT species are responsible for short wavelength emission bands which can compete with the keto tautomer, and evidence of this conformational equilibrium in the ground state can

* Corresponding authors. Tel.: +55 51 3308 6299; fax: +55 51 3308 7304.
E-mail addresses: rodembusch@gmail.com, rodembusch@iq.ufrgs.br, fabiano.rodembusch@ufrgs.br (F.S. Rodembusch), leandra.campo@ufrgs.br (L.F. Campo).

http://dx.doi.org/10.1016/j.dyepig.2014.04.024
0143-7208/

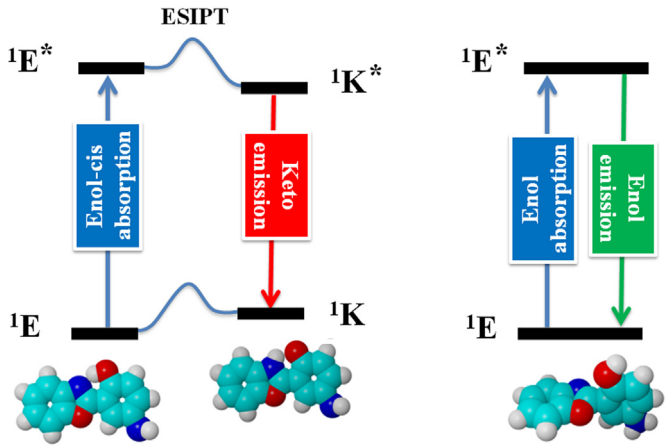

Fig. 1. Simplified photophysics of the ESIPT mechanism illustrated by the enol-*cis* conformer from the 2-(5′-amino-2′-hydroxyphenyl)benzoxazole (left). A normal emission from an enol open conformer was also presented for comparison (right).

be related to the dual fluorescence emission of these compounds [22].

This work described the synthesis of new lipophilic ESIPT dyes, their photophysical behaviour in solution and their efficiency as membrane probes after incorporation into liposomes and ethosomes. Ethosomes are vesicular systems embodying ethanol in relatively high concentrations, and are very efficient at enhancing the skin permeation of a number of drugs as already reported in the literature [23]. Additionally, the partition coefficient (K_p) of these probes was calculated and discussed.

2. Experimental

2.1. Materials and methods

All reagents were obtained from Aldrich and used without further purification. Chicken egg L-α-phosphatidylcholine (ECPC), 1,2-dipalmitoyl-*sn*-glycero-3-phosphocholine (DPPC) and 1,2-dioleoyl-*sn*-glycero-3-phosphocholine (DOPC) were purchased from Avanti Polar Lipids, Inc. and used without purification. Chromatographic purification of products was accomplished using 230–400 mesh silica gel and thin-layer chromatography (TLC) was performed on 0.20 mm silica gel plates (Whatman Al Sil G/UV). All solvents were used as received or purified using standard procedures, while spectroscopic grade solvents (Merck or Aldrich) were used for fluorescence and UV–Vis measurements. Melting points were measured with a Thermolyne apparatus and were uncorrected. ^1H and ^{13}C NMR spectra were recorded on a Varian Inova 300 MHz spectrometer or Varian VNMRs 300 MHz spectrometer. The chemical shifts were expressed as δ (ppm) relative to tetramethylsilane (TMS) as the internal standard and using $CDCl_3$ or CF_3COOD (as the solvents) at room temperature. Data for ^1H NMR were reported as follows: multiplicity (s = singlet, d = doublet, t = triplet, m = multiplet), integration, coupling constant (Hz) and assignment. Data for ^{13}C APT were reported in terms of chemical shift (ppm) and infrared spectra were recorded on a Varian 640-IR using KBr pellets. Elemental analysis was performed in a Perkin–Elmer CHN 2400, UV–Vis absorption spectra were determined using a Shimadzu UV-2450 spectrophotometer and steady state fluorescence spectra were measured using a Shimadzu spectrofluorometer model RF-5301PC. Spectrum correction was performed to allow measurements of true spectra by eliminating instrumental responses such as wavelength characteristics of the monochromator or detector using Rhodamine B as an external standard (quantum counter). All experiments were performed at room temperature (25 °C) at a 10^{-5} M concentration (Electronic Supporting Information, Table ESI1). The quantum yield of fluorescence (Φ_{fl}) was measured at 25 °C using spectroscopic grade solvents in the optical dilute methodology. Quinine sulfate (Riedel) was used as the quantum yield standard [24].

2.2. Synthesis

2.2.1. 2-(5′-Amino-2′-hydroxyphenyl)benzoxazole (**3**)

The aminobenzoxazole **3** was obtained in a condensation reaction of equimolar amounts of 5-aminosalicylic acid (**1**) and 2-aminophenol (**2**) in polyphosphoric acid (PPA) at 180 °C for 5 h, followed by TLC using dichloromethane as the eluent. The reaction mixture was poured onto ice, the precipitate filtered, neutralized with $NaHCO_3$ (20%) and dried at 60 °C. The material was purified by column chromatography (eluted with dichloromethane) to yield the corresponding aminobenzoxazole **3**. Yield: 74%. Yellow powder, m.p.: 174–175 °C (Lit. 173–175 °C [25]). FTIR (KBr, cm^{-1}): 3410 (ν_{as} NH_2); 3330 (ν_s NH_2), 1630 and 1545 (ν C=C). ^1H NMR ($CDCl_3$, 300 MHz, TMS): δ (ppm) = 10.94 (broad s, 1H, OH), 7.83–6.74 (m, 7H, Ar–H), 3.54 (broad s, 2H, NH_2). Anal. Calcd. for $C_{13}H_{10}N_2O_2$: C, 69.02; H, 4.46; N, 12.38%; Anal. Found: C, 69.06; H, 4.56; N, 12.06%.

2.2.2. Synthesis of 2-(5′-N-octylamino-2′-hydroxyphenyl) benzoxazole (**4**)

Compound **3** (0.61 g, 2.65 mmol), iodooctane (1.27 g, 5.3 mmol) and potassium carbonate (0.36 g, 2.65 mmol) in 2-butanone (15 mL) were mixed and stirred for 18 h at reflux temperature. The solvent was removed under reduced pressure and a dark-brown oil was obtained which was purified by column chromatography using chloroform: hexane (1:1) as the eluent. Yield: 45%. Dark-yellow crystals, m.p.: 92–94 °C. FTIR (KBr, cm^{-1}): 3440 (ν OH), 3400 (ν NH), 2930 (ν C–H), 2840 (ν C–H). ^1H NMR ($CDCl_3$, 300 MHz, TMS): δ (ppm) = 10.89 (broad s, 1H, OH), 7.75–7.67 (m, 1H, Ar–H), 7.63–7.55 (m, 1H, Ar–H), 7.40–7.32 (m, 2H, Ar–H), 7.24–7.19 (m, 1H, Ar–H), 7.01–6.95 (m, 1H, Ar–H), 6.83–6.76 (m, 1H, Ar–H), 3.14 (t, 2H, N–CH), 2.84 (broad s, 1H, NH), 1.64 (m, 3H, CH), 1.34 (m, 8H, CH), 0.89 (t, 3H, CH). ^{13}C NMR ($CDCl_3$, 75.4 MHz, TMS): δ (ppm) = 162.9, 152.0, 149.1, 140.7, 140.2, 125.38, 124.9, 121.2, 119.2, 118.1, 110.6, 110.3, 109.8, 44.9, 31.7, 29.5, 29.3, 29.0, 27.13, 22.6, 14.0. Anal. Calcd. for $C_{21}H_{26}N_2O_2$: C, 74.25; H 7.96; N 7.90%; Anal. Found: C, 74.55; H, 7.69; N, 8.28%.

2.2.3. Synthesis of 2-(5′-N-cis-9-octadecenamide-2′-hydroxyphenyl)benzoxazole (**5**)

Oleic acid (0.497 g, 1.76 mmol), *N,N′*-dicyclohexylcarbodiimide (DCC) (0.439 g, 2.13 mmol) and a catalytic amount of de 4-*N,N*-dimethylaminopyridine (DMAP) in dry dichloromethane (30 mL) were mixed and the reaction stirred under argon for 3 h at room temperature (25 °C). To this reaction mixture, the benzoxazole precursor **3** (0.400 g, 1.76 mmol) was added and stirred overnight at room temperature. The precipitate, mostly composed by DCU, was removed by filtration and washed with dichloromethane (3 × 20 mL). The organic layers containing the product were combined, washed with water (4 × 50 mL), dried ($MgSO_4$), concentrated under reduced pressure and the residue purified by column chromatography, eluting with dichloromethane. Yield: 50%. White powder, m.p.: >300 °C. FTIR (KBr, cm^{-1}): 3281 (ν NH), 2921 (ν C–H), 2853 (ν C–H), 1709 (ν C=C), 1648 (ν C=O), 1531 (ν C=C), 1451 (ν C=C), 1250 (ν C–N). ^1H NMR ($CDCl_3$, 300 MHz, TMS): δ (ppm) = 11.31 (broad s, 1H, OH), 8.35 (s, 1H, NH), 7.73–7.66 (m, 1H, Ar–H), 7.60–7.53 (m, 1H, Ar–H), 7.47–7.32 (m, 4H, Ar–H), 7.08–

7.02 (m, 1H, Ar–H), 5.34 (t, 2H, C=C–H), 2.39 (*t*, 2H, COC–H), 2.00 (t, 2H, C–H), 1.76 (m, 2H, C–H), 1.32 (m, 25H, C–H), 0.88 (t, 3H, C–H). ^{13}C NMR ($CDCl_3$, 75.4 MHz, TMS): δ (ppm) = 171.6, 162.5, 155.5, 149.1, 139.9, 130.1, 130.0, 129.7, 126.2, 125.5, 125.0, 119.2, 118.8, 117.7, 110.8, 110.3. Anal. Calcd. for $C_{31}H_{42}N_2O_3$: C, 75.88; H, 8.63; N, 5.71%; Anal. Found: C, 76.34; H, 9.33; N, 5.93%.

2.2.4. Synthesis of 2-(5′-N-octadecanamide-2′-hydroxyphenyl) benzoxazole (**6**)

Lipophilic derivative **6** was prepared using two different methodologies. Method 1: Stearic acid (0.629 g, 2.21 mmol), *N*-(3-dimethylaminopropyl)-*N*′-ethylcarbodiimide hydrochloride (EDCI) (0.429 g, 2.21 mmol) and a catalytic amount of 4-*N*,*N*-dimethylaminopyridine (DMAP) in dry dichloromethane (30 mL) were stirred under argon for 3 h at room temperature (25 °C), **3** (0.500 g, 2.21 mmol) added and stirred overnight at room temperature. The solid was separated by filtration and TLC analysis showed no product in filtrate. The residue, composed mainly of urea and product, was suspended in 1 L of water, stirred for 12 h and pure product obtained by filtration. Method 2: In a round-bottom flask equipped with a condenser, stearic acid (0.500 g, 1.76 mmol) and thionyl chloride (0.500 mL, 6.85 mmol) were stirred under reflux for 6 h. The excess thionyl chloride was removed by evaporation followed by the addition of **3** (0.400 g, 1.76 mmol) and triethylamine (200 μL) in dry dichloromethane (20 mL). The reaction was stirred overnight at room temperature (25 °C), the precipitate filtered and washed with water to yield compound **6**. Yield: 50%. White powder, m.p. >300 °C. FTIR (KBr, cm^{-1}): 3295 (ν NH), 2921 (ν C–H), 2853 (ν C–H), 1648 (ν C=O), 1540 (ν C=C), 1470 (ν C=C), 1256 (ν C–N). ^{1}H NMR (CF_3COOD, 300 MHz, TMS): δ (ppm) = 11.66 (broad s, 1H, OH), 8.87 (s, 1H, NH), 8.21–8.10 (m, 2H, Ar–H), 8.07–7.92 (m, 4H, Ar–H), 7.62–7.54 (m, 1H, Ar–H), 2.89 (t, 2H, COC–H), 2.09 (m, 2H, C–H), 1.78–1.41 (m, 28H, C–H), 1.09 (t, 2H, C–H). ^{13}C NMR (CF_3COOD, 75.4 MHz, TMS): δ (ppm) = 178.8, 161.3, 156.8, 148.0, 133.9, 130.2, 129.6, 128.9, 127.6, 123.7, 118.3, 115.2, 112.3, 105.9, 36.4, 31.6, 29.3, 29.3, 29.3, 29.3, 29.2, 29.0, 29.0, 28.8, 28.8, 25.8, 22.2, 12.5. Anal. Calcd. for $C_{31}H_{44}N_2O_3$: C, 75.57; H, 9.00; N, 5.59%; Anal. Found: C, 75.54; H, 8.67; N, 5.67%.

2.3. Labelling of liposome for photophysical study

The liposomes were prepared based on a previously published methodology [26,27], where stock solutions of the lipophilic dyes **4**–**6** were prepared in chloroform ($\sim 10^{-5}$ M) in which the lipid (ECPD, DPPC or DOPC) (50–60 mg) was solubilized (round-bottom flask). After total solubilization of the lipid, the solvent was removed under reduced pressure, yielding a thin film deposited on the inner walls of the round-bottomed flask. The films were hydrated with 4 mL water, dispersed by stirring and sonicated for 30 min.

2.4. Labelling of ethosome for photophysical study

Ethosomes were prepared based on published methodologies [23,28]. Ethosomes were composed of 1% lipid, 1% dye, 40% ethanol and 58% water (w/w) where 1 mg of dye (**4**, **5** or **6**) and lipid (ECPD, DPPC or DOPC) were solubilized in ethanol (40 mL) and water (60 mL) was added with stirring. The mixture was stirred for an additional 10 min.

2.5. Labelling of liposomes for partition experiments

The partition experiments were performed as previously described [29–31]. Stock solutions of each dye in methanol (5.0×10^{-5} M) and ECPC, DPPC and DOPC liposomes were prepared. Partition experiment were performed using a titration method where the dye solution (1 mL) was added to different concentrations of liposomes (1 mL) in water (pH 7.0) to yield solutions with phospholipid: dye ratios of 1–50. After the addition of dye, the solutions was kept at 20 °C for 1 h before experiments. Blank solutions were prepared by adding pure methanol instead of dye to the liposome solutions.

3. Results and discussion

3.1. Synthesis

The aminobenzazole **3** was prepared using a previously described methodology [25], which involved the condensation of an equimolar amount of 5-aminosalicylic acid (**1**) with the o-substituted aniline **2** in polyphosphoric acid (PPA) (Scheme 1).

The lipophilic derivatives **4**–**6** were prepared according to Scheme 2. The procedure for the synthesis of dye **4** consisted of a bimolecular nucleophilic reaction using iodooctane as the alkylating agent in 2-butanone [32,33]. Derivatives **5** and **6** were prepared by the Steglich esterification method using dicyclohexylcarbodiimide and 4-*N*,*N*-dimethylaminopyridine as reactants [34]. Dye **5** was prepared by the reaction of **3** with oleic acid using DCC/DMAP as coupling reagents [35,36]. Despite the use of deactivated carboxylic acid, this methodology provided good yields, though the urea (by-product) was difficult to remove. As the urea could not be removed by washing, column chromatography was performed twice to obtain product free from urea. A similar strategy was applied to **6**, modifying the coupling agent, as the by-product formed by EDCI was water-soluble [37], where urea was removed by stirring the crude product with water followed by filtration. An alternative methodology was also tested, where the carboxylic acid was converted in acyl chloride [38] using $SOCl_2$ (Method 2), followed by reaction with **3** to form the desired amide lipophilic dye **6** at a low yield.

3.2. Photophysical characterization of the lipophilic dyes

The UV–Vis absorption spectra of lipophilic dyes **4**–**6** are shown in Fig. 2 and relevant data from UV–Vis absorption spectroscopy are presented in Table 1.

Dyes **4**–**6** had absorption maxima at 385, 344 and 343 nm, respectively. The molar absorptivity coefficient ε values, as well as the calculated radiative rate constant (k_e^0) for all dyes indicated spin allowed electronic transitions, which could be related to π–π^* transitions. No significant solvatochromism in the ground state was observed. Dye **4** had an absorption maximum redshifted compared to the precursor **3** [22], indicating that alkylation of the amino group enhanced the electron-donating effect. It is well-known that a qualitative understanding of the effects of substituents on the position of the UV–Vis spectrum can be considered by classifying the substituents into electron-donating and electron-withdrawing groups. Since dyes **5** and **6** possess electron-withdrawing amide moieties, a decrease in the π-system length takes place through resonance, and shifts the absorption maxima to shorter wavelengths (when compared to **3**). Additionally, the intense absorption

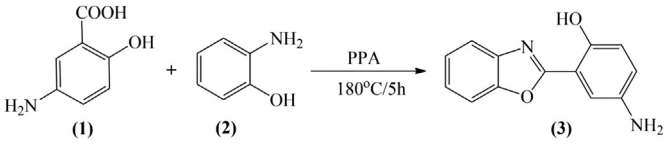

Scheme 1. Synthesis of the 2-(5′-amino-2′-hydroxyphenyl)benzoxazol (**3**).

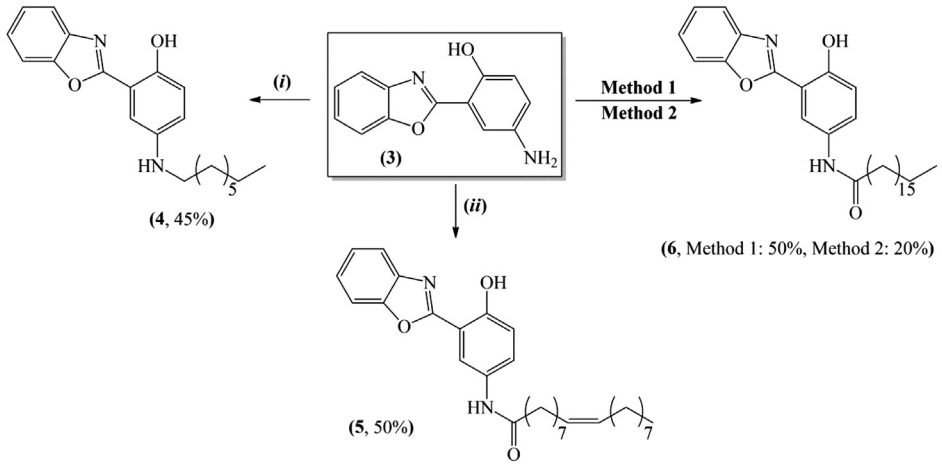

Scheme 2. Synthesis of the lipophilic benzoxazoles **4**–**6**, where (i) iodooctane, K_2CO_3, 2-butanone, reflux, 18 h; (ii) oleic acid, dicyclohexylcarbodiimide (DCC), 4-*N*,*N*-dimethylaminopyridine (DMAP), dichloromethane, overnight; Method 1: stearic acid, *N*-(3-dimethylaminopropyl)-*N*′-ethylcarbodiimide hydrochloride (EDCI), 4-*N*,*N*-dimethylaminopyridine (DMAP), dichloromethane, overnight; Method 2: stearic acid, $SOCl_2$, reflux; NEt_3, dichloromethane, overnight.

bands observed at 280–310 nm was observed in similar compounds [22] and can be associated to the absorption of the benzoxazole moiety [39].

The normalized fluorescence emission spectra of lipophilic dyes **4**–**6** are presented in Fig. 3, where emission curves were obtained using the absorption maxima as the excitation wavelength, while relevant data from fluorescence emissions are summarized in Table 2.

At least for one solvent, the fluorescence spectra showed a dual emission (as expected), since it is known that the ESIPT mechanism in amino derivatives is dependent on solvent polarity [22]. The emission at short wavelengths could be ascribed to normal emission from an enol conformer ($^1E^*$), while the redshifted emission located in the green–yellow region was related to the keto tautomer ($^1K^*$), which arises from the ESIPT in the excited state. These results indicated the photophysics of these compounds were complex, and the results from one benzoxazole fluorophore cannot be extended to parent compounds, as usually observed for classical aromatic photoactive dyes with different substituents [40]. In ethanol, for instance, the precursor **3** had a single emission band due to stabilization in the ground state of an enol conformer which does not exhibit phototautomerism in the excited state. The derivatization of this compound seemed to affect the photophysics of the fluorophore benzoxazole, since **5** and **6** in the same solvent showed ESIPT bands at longer wavelengths, indicating ethanol could stabilize the enol *cis* conformer which would transfer a proton in the excited state to produce the keto tautomer.

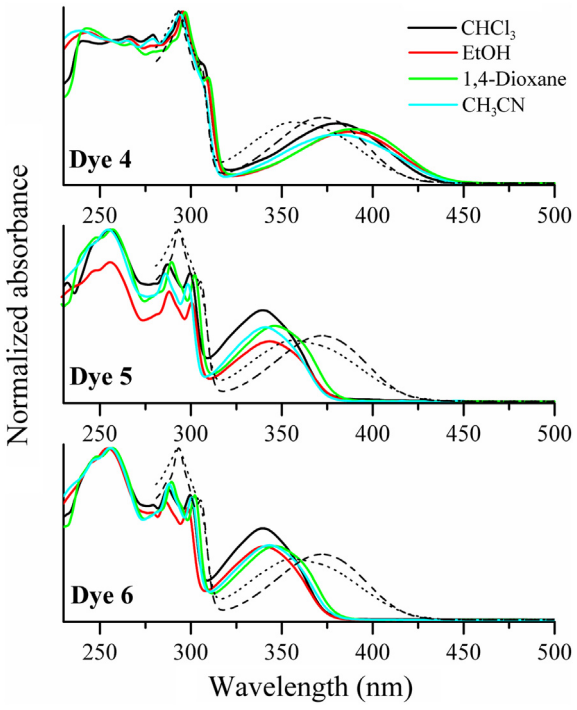

Fig. 2. Normalized UV–Vis absorption spectra of the lipophilic ESIPT dyes **4**–**6**. The UV–Vis spectra of the precursor **3** in MeCN (dash line) and EtOH (dot line) was also presented for comparison.

3.3. Photophysical characterization of the liposomes and ethosomes

Fig. 4 shows the electronic absorption spectra of ESIPT dyes **4**–**6** in ECPC, DPPC and DOPC liposomes and ethosomes. Upon incorporation, the absorption maxima of lipophilic dyes **5** and **6** did not significantly change shape and spectral position. Additionally, the phenylbenzoxazole derivatives can possess two distinct absorption regions, the first at 280–310 nm (ascribed to the benzoxazole chromophore) and the other above 330 nm (π-extended

Table 1
Relevant photophysical data from the UV–Vis spectra of the lipophilic dyes **4**–**6**, where λ_{abs} is the absorption maxima, ε is the molar absorptivity coefficient, f_e is the calculated oscillator strength, k_e^0 is the calculated radioactive rate constant and $\nu_{0\text{-}0}$ is the frequency of purely electronic transition.

Dye	Solvent	λ_{abs} (nm)	ε (M^{-1} cm^{-1})	f_e	k_e^0	$\nu_{0\text{-}0}$ (cm^{-1})
4	Chloroform	380	6220	0.12	8.58×10^7	23,294
	Ethanol	380	3189	0.07	4.65×10^7	22,743
	1,4-Dioxane	391	11,288	0.22	1.47×10^8	22,541
	Acetonitrile	388	9661	0.20	1.30×10^8	22,497
5	Chloroform	341	8246	0.17	1.46×10^8	26,606
	Ethanol	342	2890	0.04	3.34×10^7	26,618
	1,4-Dioxane	348	14,706	0.26	2.18×10^8	26,128
	Acetonitrile	343	21,961	0.13	1.09×10^8	26,377
6	Chloroform	340	24,198	0.45	3.91×10^8	26,658
	Ethanol	342	18,899	0.32	2.76×10^8	26,521
	1,4-Dioxane	348	17,488	0.30	2.49×10^8	26,111
	Acetonitrile	343	22,759	0.16	1.32×10^8	26,323

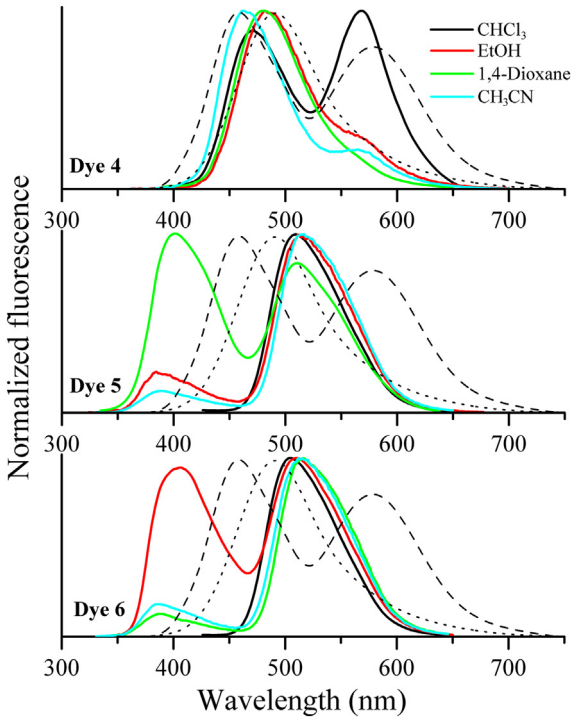

Fig. 3. Normalized fluorescence emission spectra of the lipophilic ESIPT dyes **4**–**6** (10^{-5} M). The fluorescence emission spectra of the precursor **3** in MeCN (dash line) and EtOH (dot line) was also presented for comparison.

chromophore phenylbenzoxazole) [22,41], and the difference in absorption band intensities can be associated with a difference in planarity in some dyes [22,42]. The observed changes in absorption band intensities for dyes **4**–**6** incorporated in liposomes and ethosomes, can yield interesting results (as follows).

An empirical ratio could be calculated, so-called planarity factor F_p by the equation $F_P = I_{bz}/I_{max}$, where I_{bz} is the intensity of the absorption band located between 280 and 310 nm and I_{max} is the intensity of the absorption maxima, where the lower the F_P the higher the planarity of the π-extended chromophore. Considering the non-normalized absorption spectra (Electronic Supporting Information, Figs. ESI16–18), dyes **5** and **6** had a value of $F_P \sim 1.6$, and dye **4** had a calculated value of ~3.2 (Electronic Supporting Information, Tables ESI3–5). This difference indicated that in solution, dye **4** tended to be less planar than dyes **5** and **6**. In liposomes and ethosomes (Fig. 4), dyes **5** and **6** had lower F_P (~1) values (similar to those observed in solution), while dye **4** exhibited a very particular photophysical behaviour. In liposomes, the average value for F_P was higher (~2) than those observed for the parent compounds, while in ethosomes, despite having the same absorption region, the spectra changed drastically and the planarity factor increased to an average value of ~6. In ECPC ethosomes, F_P reached the maximum value of 11.6, which indicated the phenyl ring was not conjugated with the benzoxazole backbone in ethosomes. Thus, the absorption spectrum may be described by two independent absorption bands for each subunit, as observed for similar structures [41]. These data suggested the intensity of the higher absorption maxima was reinforced conjugation enabled by the intramolecular hydrogen bond.

The fluorescence emission curves of lipophilic ESIPT dyes **4**–**6** in liposomes and ethosomes are presented in Fig. 5. The curves were obtained using the absorption maxima for each dye as the excitation wavelength and relevant data from the liposome and ethosome photophysical studies are summarized in Table 3.

Dyes **5** and **6** had one narrow emission band with a very regular shape and location in liposomes and ethosomes (~500 nm, with a Stokes' shift ~9500 cm^{-1}) ascribed to the ESIPT mechanism. Although it is well-known the ESIPT mechanism in benzazoles is dependent on solvent [22] and polarity microenvironments [43], the surroundings provided by the different phospholipids in liposomes or ethosomes, as well as the alkyl chain length of dyes **5** and **6**, appeared to play a fundamental role in the photophysics of the

Table 2
Relevant photophysical data from the fluorescence emission spectra of the lipophilic dyes **4**–**6**, where λ_{em} is the emission maxima, $\Delta\lambda_{ST}$ is the Stokes' shift and Φ_{fl} is the quantum yield of fluorescence.

Dye	Solvent	Enol conformer		Keto tautomer		Φ_{fl} ($\times 10^{-2}$)
		λ_{em} (nm)	$\Delta\lambda_{ST}$ (nm/cm^{-1})	λ_{em} (nm)	$\Delta\lambda_{ST}$ (nm/cm^{-1})	
4	Chloroform	471	91/5084.8	568	188/8710.2	2.31
	Ethanol	481	101/5525.8	–	–	1.12
	1,4-Dioxane	464	73/4023.7	587	196/8539.6	0.41
	Acetonitrile	486	98/5197.1	587	199/8737.4	0.24
5	Chloroform	–	–	509	168/9679.1	1.51
	Ethanol	403	61/4425.9	510	168/9631.9	0.75
	1,4-Dioxane	391	43/3160.2	518	170/9430.6	0.83
	Acetonitrile	391	48/3579.1	516	173/9774.7	1.11
6	Chloroform	–	–	505	165/10,031.9	1.90
	Ethanol	406	64/4609.3	511	169/9859.9	0.67
	1,4-Dioxane	390	42/3094.6	516	168/9355.8	0.71
	Acetonitrile	388	45/3381.3	516	173/9774.7	0.43

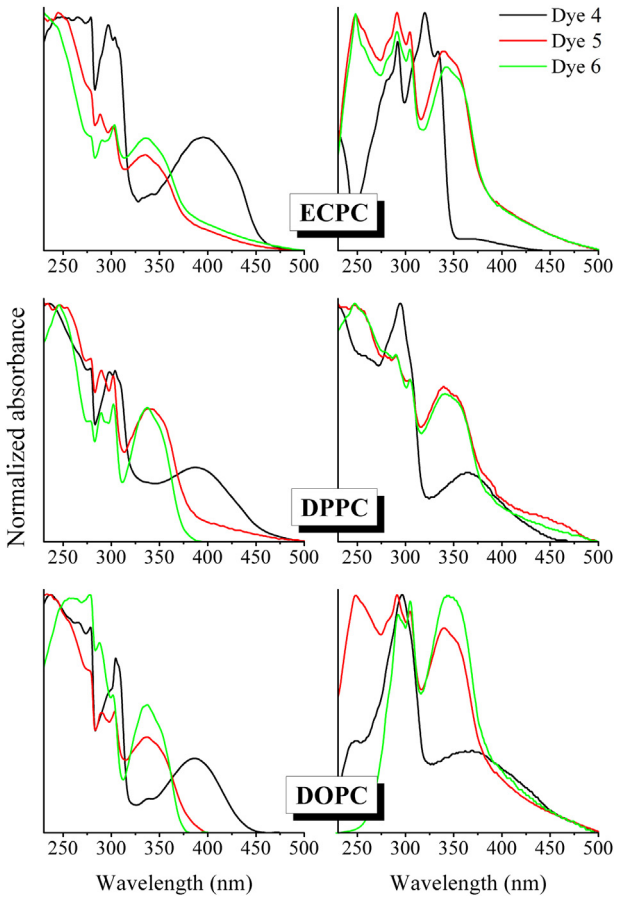

Fig. 4. Normalized UV–Vis absorption spectra of the lipophilic ESIPT dyes **4**–**6** in liposomes (left) and ethosomes (right), where ECPC, DPPC and DOPC are the phospholipids egg chicken L-α-phosphatidylcholine, 1,2-dipalmitoyl-*sn*-glycero-3-phosphocholine and 1,2-dioleoyl-*sn*-glycero-3-phosphocholine, respectively.

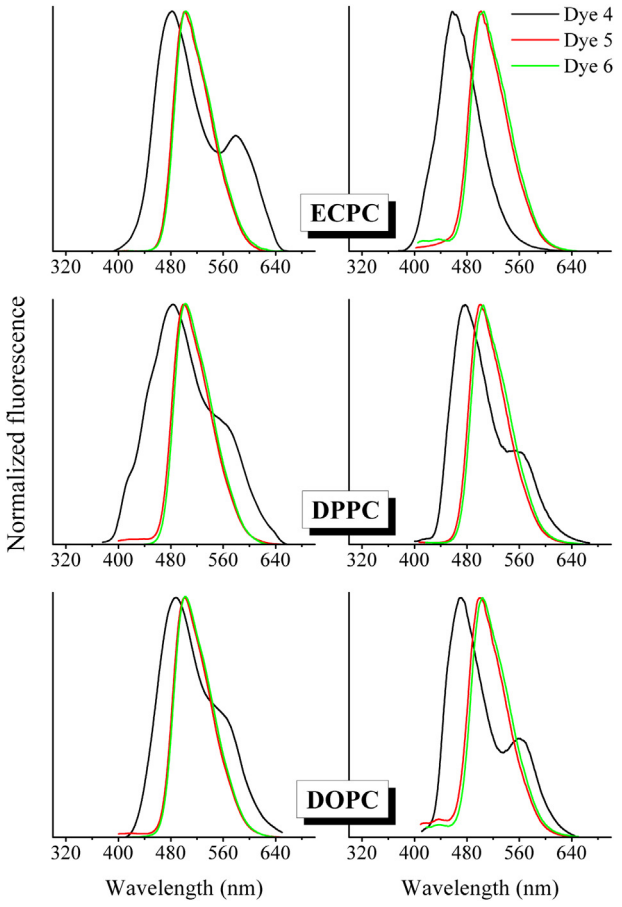

Fig. 5. Normalized fluorescence emission spectra of the lipophilic ESIPT dyes **4**–**6** in liposomes (left) and ethosomes (right), where ECPC, DPPC and DOPC are the phospholipids egg chicken L-α-phosphatidylcholine, 1,2-dipalmitoyl-*sn*-glycero-3-phosphocholine and 1,2-dioleoyl-*sn*-glycero-3-phosphocholine, respectively.

Table 3
Relevant photophysical data from the UV–Vis absorption and fluorescence emission spectra of the liposomes and ethosomes, where λ_{abs} and λ_{em} are the absorption and emission maxima, respectively and $\Delta\lambda_{ST}$ is the Stokes' shift.

Dye	Phospholipid	λ_{abs} (nm)	Fluorescence emission			
			Enol conformer		Keto tautomer	
			λ_{em} (nm)	$\Delta\lambda_{ST}$ (nm/cm^{-1})	λ_{em} (nm)	$\Delta\lambda_{ST}$ (nm/cm^{-1})
Liposomes						
4	ECPC	396	482	86/4505.6	581	185/8040.8
	DPPC	391	482	91/4828.6	563	172/7813.5
	DOPC	387	487	100/5305.9	559	172/7950.7
5	ECPC	336	–	–	502	166/9841.6
	DPPC	343	–	–	502	159/9234.2
	DOPC	338	–	–	502	164/9665.5
6	ECPC	337	–	–	502	165/9753.3
	DPPC	338	–	–	502	164/9665.5
	DOPC	338	–	–	502	164/9665.5
Ethosomes						
4	ECPC	379	459	80/4598.7	–	–
	DPPC	366	477	111/6358.0	563	197/9560.4
	DOPC	373	473	100/5668.0	565	192/9110.5
5	ECPC	339	–	–	503	164/9617.8
	DPPC	340	–	–	503	163/9531.0
	DOPC	341	–	–	501	160/9365.4
6	ECPC	342	–	–	503	161/9359.1
	DPPC	338	–	–	503	165/9705.1
	DOPC	348	–	–	501	153/8775.6

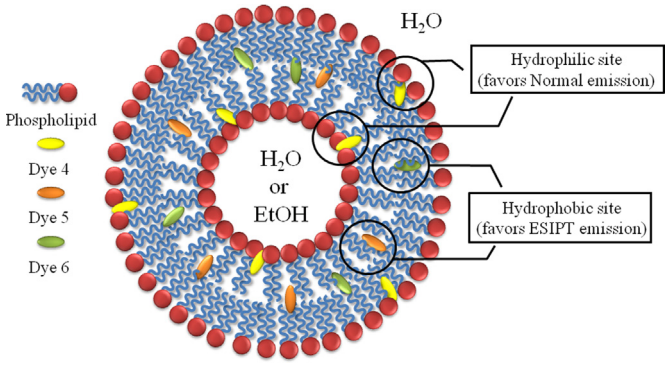

Scheme 3. Pictorial representation of the lipophilic dyes **4**–**6** into the lipid bilayer of liposomes (H_2O in the interior) and ethosomes (ethanol in the interior), based on the fluorescence emission profile of the lipophilic dyes.

benzoxazole fluorophore, which allowed these dyes to experience an apolar environment. These results indicated the dyes were inserted into the lipid bilayer without contact with the water or ethanolic surroundings (Scheme 3). On the other hand, dye **4** had a blueshifted band (compared to dyes **5** and **6**) located around 477 nm, ascribed to the normal emission ($\Delta\lambda_{ST}$ ~5211 cm^{-1}), despite the emission band at long wavelengths (~566 nm) being related to the ESIPT mechanism. The photophysical behaviour indicated that unlike the parent compounds, dye **4** experienced a polar environment, which showed this fluorophore was located in a more hydrophobic environment (Scheme 3) and may be associated with the size of the alkyl chains of the dyes. Dyes **5** and **6** have longer alkyl chains and were more similar to the lipid backbone than dye **4**, and the intermolecular van der Waals interactions were favoured, keeping the dyes within the tangle of alkyl chains. Additionally, stronger interactions between **5** and **6** and the phospholipids (absent in dye **4**) existed, since ECPC, DPPC and DOPC (Electronic Supporting Information, Figs. ESI13–15) contained ester groups in their structures which could be responsible for the photophysical behaviour, and could present as dipole–dipole and hydrogen bond interactions with the amides **5** and **6**.

3.4. Fluorescence titration study

Fluorescence titration experiments were performed to study the influence of phospholipid concentration [PL] (mol/L) on the fluorescence intensity maxima of dyes. In the presence of phospholipid, the fluorescence intensity of dye **6** remained constant (Fig. 6), not seen in the absence of the phospholipid (also observed for dye **5**, Electronic Supporting Information, Figs. ESI19–21). These results indicated that for the phospholipid concentrations (mM) studied, these dyes interacted strongly with phospholipids, as at the lowest concentration, the fluorescence intensity reached the maximum value (maintained up to 2.5 mM), which was different from other ESIPT dyes [31].

However, dye **4** had a fluorescence intensity which was dependent on phospholipid concentration [PL] (Fig. 7), also seen for DPPC and DOPC (but at lower concentrations, 1.0–2.5 mM) (Electronic Supporting Information, Figs. ESI22 and 23). Additionally, the enhanced fluorescence intensity of dye **4** exhibited saturation at ~1 mM PL (Fig. 8, top).

The partition coefficients (K_p) of dye **4** in ECPC, DPPC and DOPC phospholipids were calculated from the slope of the double reciprocal linear plot of $1/F$ *vs.* $1/[PC]$ according to $1/F = 55.6/(K_pF_{max}[PC]) + 1/F_{max}$, where F_{max} was the maximum fluorescence resulting from total probe incorporation into the membrane (Fig. 8,

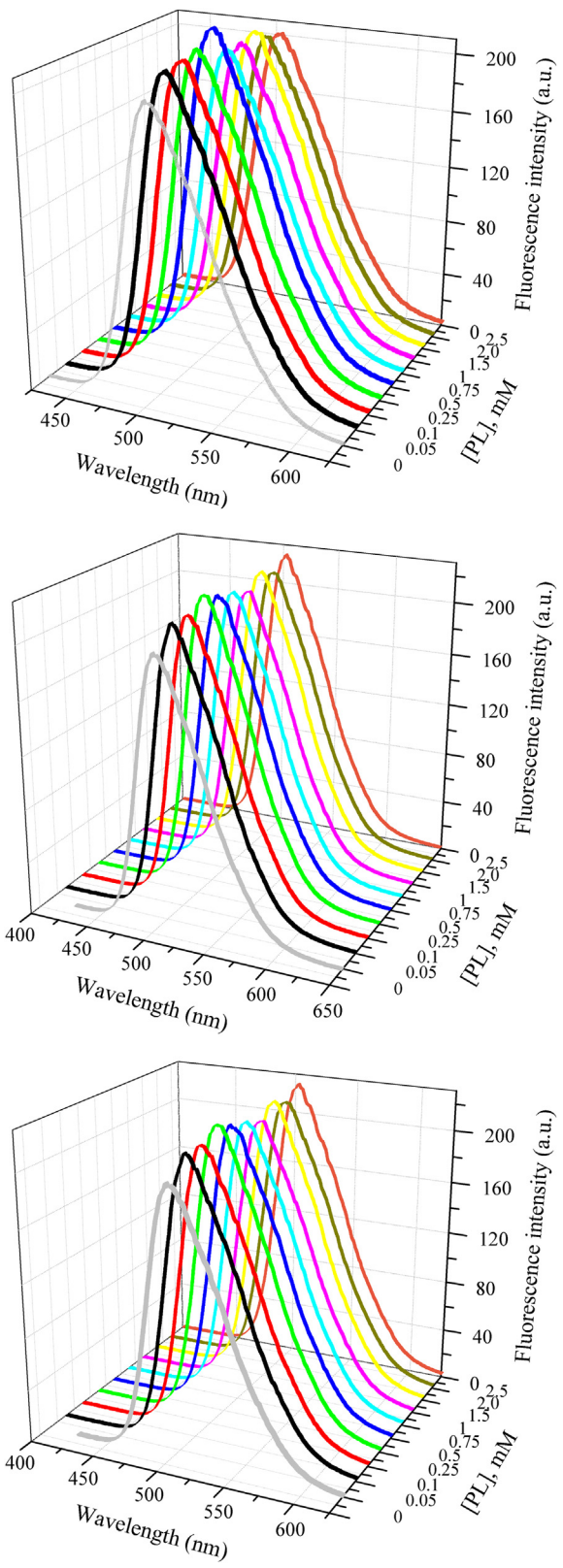

Fig. 6. Fluorescence emission spectra of dye **6** in ECPC (top), DPPC (middle) and DOPC (bottom) phospholipids for a concentration range of 0.05–2.5 mM at 25 °C. Dye **6** in absence of phospholipids was also presented for comparison (light grey line).

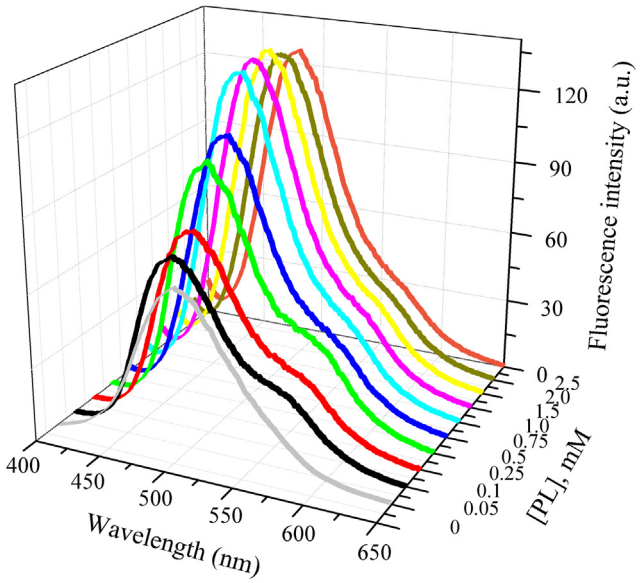

Fig. 7. Fluorescence emission spectra of dye **4** in ECPC for a concentration range of 0.05–2.5 mM at 25 °C. Dye **4** in absence of phospholipids was also presented for comparison (light grey line).

bottom) [30,31]. From the slope and $1/F$ intercepts of this linear plot, the K_p was found to be 6.67×10^5, 7.30×10^5 and 7.04×10^5 for ECPC, DPPC and DOPC, respectively, at 25 °C with an R^2 ~1 (Electronic Supporting Information, Table ESI6). The partition coefficient values found in this work were higher than those found in the literature for ESIPT dyes [31,44], likely due to better interactions between the dye and PC allowed by the alkyl chains.

4. Conclusions

In conclusion, three new fluorescent lipophilic dyes (**4**–**6**) were synthesized from an ESIPT fluorescent precursor, and used to create photoactive liposomes and ethosomes prepared from chicken egg L-α-phosphatidylcholine (ECPC), 1,2-dipalmitoyl-*sn*-glycero-3-phosphocholine (DPPC) and 1,2-dioleoyl-*sn*-glycero-3-phosphocholine (DOPC). The dyes absorbed in the UV region (~340–390 nm) which was related to π–π* transitions, where no significant solvatochromism in the ground state was observed and dual fluorescence emissions in the violet–yellow regions were seen. The emission band at short wavelengths could be related to normal emission from an enol conformer ($^1E^*$), and the long wavelength, located in the green–yellow region related to the keto tautomer ($^1K^*$), which arose from the ESIPT in the excited state. The lipophilic dyes **5** and **6** exhibited one narrow emission band with a very regular shape and location in liposomes and ethosomes ascribed to the ESIPT mechanism, which indicated the surroundings provided by the different phospholipids seemed to play a fundamental role in the photophysics of these dyes, creating an apolar environment. On the other hand, dye **4** seemed to be located in a polar environment which suggested the fluorophore was located in a more hydrophobic medium. Fluorescence titration experiments performed to study the influence of the phospholipid concentration on the fluorescence intensity indicated the partition coefficient values obtained for dye **4** was higher than those found in the literature for ESIPT dyes, and may be due to better interaction between dye and phospholipids (ascribed to the alkyl chain present). These data suggested a model for the interaction between lipophilic ESIPT dyes and some liposomes/ethosomes which

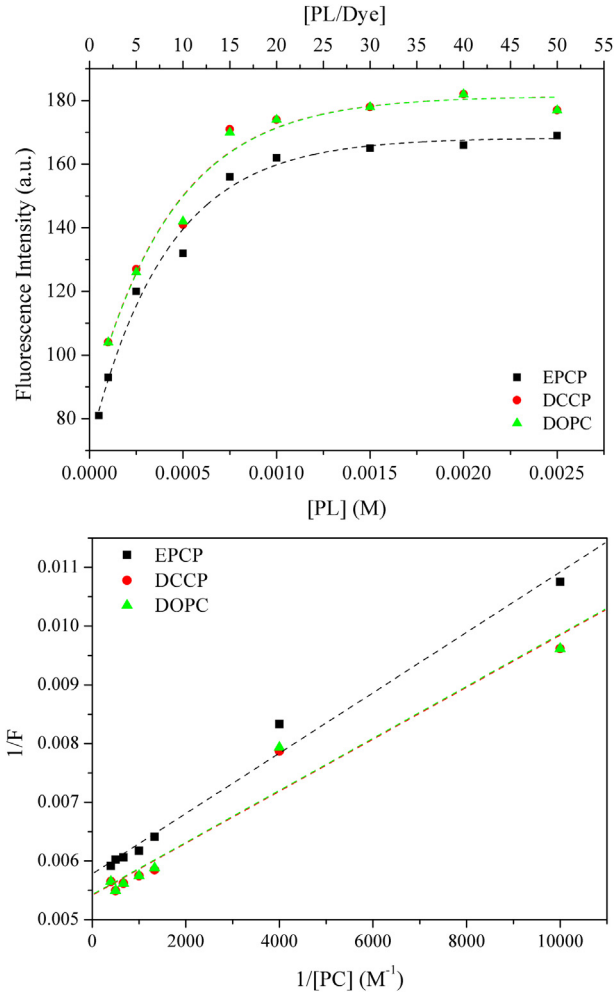

Fig. 8. Plot of fluorescence intensity (F) *vs.* [PL] of dye **4** at 25 °C (top) and double reciprocal plot of 1/F *vs.* 1/[PL] of dye **4** in different liposomes for a concentration of lipid in the range 0.05–2.5 mM at 25 °C (bottom).

characterized these new fluorescent probes in membrane environments.

Acknowledgements

We are grateful to CNPq, Coordenação de Aperfeiçoamento de Pessoal de Nível Superior and Instituto Nacional de Inovação em Diagnósticos para a Saúde Pública (INDI-Saúde) for financial support and scholarships.

Appendix A. Supplementary data

Supplementary data related to this article can be found at http://dx.doi.org/10.1016/j.dyepig.2014.04.024.

References

[1] Bangham AD, Standish MM, Watkins JC. Diffusion of univalent ions across the lamellae of swollen phospholipids. J Mol Biol 1965;13:238–52.
[2] Laouini A, Jaafar-Maalej C, Limayem-Blouza I, Sfar S, Charcosset C, Fessi H. Preparation, characterization and applications of liposomes: state of the art. J Colloid Sci Biotech 2012;1:147–68.
[3] Bittman R, Blau L. Phospholipid-cholesterol interaction. Kinetics of water permeability in liposomes. Biochemistry 1972;11:4831–9.
[4] Szoka Jr F. Comparative properties and methods of preparation of lipid vesicles (liposomes). Annu Rev Biophys Bioeng 1980;9:467–508.
[5] Huangt CH. Studies on phosphatidylcholine vesicles. Formation and physical characteristics. Biochemistry 1969;8:344–52.
[6] Singer SJ, Nicolson GL. The fluid mosaic model of the structure of cell membranes. Science 1972;175:720–31.
[7] Edidin M. The state of lipid rafts: from model membranes to cells. Annu Rev Biophys Biomol Struct 2003;32:257–83.
[8] Sessa G, Weissmann G. Phospholipid spherules (liposomes) as a model for biological membranes. J Lipid Res 1968;9:310–8.
[9] Drummen GPC. Fluorescent probes and fluorescence (microscopy) techniques – illuminating biological and biomedical research. Molecules 2012;17:14067–90.
[10] Geddes CD, editor. Reviews in fluorescence. 2009 ed. Springer; 2007. pp. 33–51.
[11] Demchenko AP, Mély Y, Duportail G, Klymchenko AS. Monitoring biophysical properties of lipid membranes by environment-sensitive fluorescent probes. Biophys J 2009;96:3461–70.
[12] Joseph R, Lakowicz JR, editors. Topics in fluorescence spectroscopy. Biochemical applications. 1992 ed., vol. 3. Springer; February 29, 1992.
[13] Subuddhi U, Haldar S, Sankararaman S, Mishra AK. Unusual fluorescence spectral response of 1-(4-*N*,*N*-dimethylaminophenylethynyl)pyrene towards the thermotropic phase change in lipid bilayer membranes. J Photochem Photobiol A Chem 2008;200:381–7.
[14] Bergelson LD, Molotkovsky JG, Manevich YM. Lipid-specific fluorescent probes in studies of biological membranes. Chem Phys Lipids 1985;37:165–95.
[15] Kwiatek JM, Owen DM, Abu-Siniyeh A, Yan P, Loew LM, Gaus K. Characterization of a new series of fluorescent probes for imaging membrane order. PLoS One 2013;8. article: e52960.
[16] Loura LMS, Ramalho JPP. Location and dynamics of acyl chain NBD-labeled phosphatidylcholine (NBD-PC) in DPPC bilayers. A molecular dynamics and time-resolved fluorescence anisotropy study. Biochim Biophys Acta 2007;1768:467–78.
[17] Krasnowska EK, Bagatolli LA, Gratton E, Parasassi T. Surface properties of cholesterol-containing membranes detected by Prodan fluorescence. Biochim Biophys Acta 2001;1511:330–40.
[18] Lentz BR. Use of fluorescent probes to monitor molecular order and motions within liposome bilayers. Chem Phys Lipids 1993;64:99–116.
[19] Hanson GT, Hanson BJ. Fluorescent probes for cellular assays. Comb Chem High Throughput Screen 2008;11:505–13.
[20] Kwon JE, Park SY. Advanced organic optoelectronic materials: harnessing excited-state intramolecular proton transfer (ESIPT) process. Adv Mater 2011;23:3615–42.
[21] Zhao JZ, Ji SM, Chen YH, Guo HM, Yang P. Excited state intramolecular proton transfer (ESIPT): from principal photophysics to the development of new chromophores and applications in fluorescent molecular probes and luminescent materials. Phys Chem Chem Phys 2012;14:8803–17.
[22] Rodembusch FS, Leusin FP, Campo LF, Stefani V. Excited state intramolecular proton transfer in amino 2-(2′-hydroxyphenyl)benzazole derivatives: effects of the solvent and the amino group position. J Lumin 2007;126:728–34.
[23] Touitou E, Dayan N, Bergelson L, Godin B, Eliaz M. Ethosomes – novel vesicular carriers for enhanced delivery: characterization and skin penetration properties. J Control Release 2000;65:403–18. and references cited therein.
[24] Würth C, Grabolle M, Pauli J, Monika S, Resch-Genger U. Relative and absolute determination of fluorescence quantum yields of transparent samples. Nat Protoc 2013;8:1535–50.
[25] Denisova LI, Kosareva VM, Solonenko IG. Synthesis of benzoxasoles and their testing in mice with nippostrongylosis. Khimiko-Farmatsevticheskii Zhurnal 1976;10:53–6.
[26] Burns ST, Khaledi MG. Rapid determination of liposome-water partition coefficients (K_{lw}) using liposome electrokinetic chromatography (LEKC). J Pharm Sci 2002;91:1601–12.
[27] Akbarzadeh1 A, Rezaei-Sadabady R, Davaran S, Joo SW, Zarghami N, Hanifehpour Y, et al. Liposome: classification, preparation, and applications. Nanoscale Res Lett 2013;8:102–10.
[28] Barupal AK, Gupta V, Ramteke S. Preparation and characterization of ethosomes for topical delivery of aceclofenac. Indian J Pharm Sci 2010;72:582–6.
[29] Bondar OP, Rowe ES. Preferential interactions of fluorescent probe prodan with cholesterol. Biophys J 1999;76:956–62.
[30] Huang Z, Haugland RP. Partition coefficients of fluorescent probes with phospholipid membranes. Biochem Biophys Res Commun 1991;181:166–71.
[31] Chaudhuri S, Basu K, Sengupta B, Banerjee A, Sengupta PK. Ground- and excited-state proton transfer and antioxidant activity of 3-hydroxyflavone in egg yolk phosphatidylcholine liposomes: absorption and fluorescence spectroscopic studies. Luminescence 2008;23:397–403.
[32] Raimundo JM, Blanchard P, Gallego-Planas N, Mercier N, Ledoux-Rak I, Hierle R, et al. Design and synthesis of push-pull chromophores for second-order nonlinear optics derived from rigidified thiophene-based π-conjugating spacers. J Org Chem 2002;67:205–18.
[33] Fang JY, Whitaker C, Weslowski B, Chen MS, Naciri J, Shashidhar R. Synthesis and photodimerization in self-assembled monolayers of 7-(8-trimethoxysilyloctyloxy) coumarin. J Mater Chem 2001;11:2992–5.
[34] Neises B, Steglich W. Simple method for the esterification of carboxylic acids. Angew Chem Int Ed 1978;17:522–4.
[35] Sheikh MC, Takagi S, Yoshimura T, Morita H. Mechanistic studies of DCC/HOBt-mediated reaction of 3-phenylpropionic acid with benzyl alcohol and studies on the reactivities of 'active ester' and the related derivatives with nucleophiles. Tetrahedron 2010;66:7272–8.

[36] Conti P, Tamborini L, Pinto A, Sola L, Ettari R, Mercurio C, et al. Design and synthesis of novel isoxazole-based HDAC inhibitors. Eur J Med Chem 2010;45:4331–8.
[37] Valeur E, Bradley M. Amide bond formation: beyond the myth of coupling reagents. Chem Soc Rev 2009;38:606–31.
[38] Green M, Thorp DM. The mechanism of reaction of phosphorus pentachloride and thionyl chloride with carboxylic esters. J Chem Soc B Phys Org; 1967:1067–8.
[39] Passerini R. The near-ultra-violet absorption spectra of some heterocyclic compounds. Part I. Benzoxazoles. J Chem Soc; 1954:2256–61.
[40] Berlman IB. Handbook of florescence spectra of aromatic molecules. 2nd ed. Academic Press; 1971.
[41] Kim CH, Park J, Seo J, Park SY, Joo T. Excited state intramolecular proton transfer and charge transfer dynamics of a 2-(2′-hydroxyphenyl)benzoxazole derivative in solution. J Phys Chem A 2010;114:5618–29.
[42] Douhal A, Amat-Guerri F, Lillo MP, Acuña AU. Proton transfer spectroscopy of 2-(2′-hydroxyphenyl)imidazole and 2-(2′-hydroxyphenyl)benzimidazole dyes. J Photochem Photobiol A Chem 1994;78:127–38.
[43] Grando SR, Pessoa CM, Costa TMH, Gallas MR, Rodembusch FS, Benvenutti EV. Modulation of the ESIPT emission of benzothiazole type dye incorporated in silica-based hybrid materials. Langmuir 2009;25:13219–23.
[44] Shyamala T, Mishra AK. Ground- and excited-state proton transfer reaction of 3-hydroxyflavone in dimyristoylphosphatidylcholine liposome membrane. Photochem Photobiol 2004;80:309–15.